Multiresolution analysis of the two-dimensional free decaying turbulence in a pure electron plasma

2009 New J. Phys. 11 053006

(http://iopscience.iop.org/1367-2630/11/5/053006)

New Journal of Physics
The open-access journal for physics

Multiresolution analysis of the two-dimensional free decaying turbulence in a pure electron plasma

G Bettega, R Pozzoli and M Romé[1]
INFN Sezione di Milano and Dipartimento di Fisica, Università degli Studi di Milano, Via Celoria 16, I-20133 Milano, Italy
E-mail: rome@mi.infn.it

New Journal of Physics **11** (2009) 053006 (10pp)
Received 1 December 2008
Published 19 May 2009
Online at http://www.njp.org/
doi:10.1088/1367-2630/11/5/053006

Abstract. The two-dimensional (2D) freely decaying turbulence is investigated experimentally in an electron plasma confined in a Malmberg–Penning trap and studied using a wavelet-based multiresolution analysis. The coherent and incoherent parts of the flow are extracted using a recursive denoising algorithm with an adaptive self-consistent threshold. Only a small number of wavelet coefficients (but corresponding to the greatest part of the enstrophy or energy contents) turns out to be necessary to represent the coherent component. The remaining small amplitude coefficients represent the incoherent component, which is characterized by a near Gaussian vorticity PDF. Scale contributions to the measured enstrophy and energy distributions are inferred, and the results are compared with recent experiments and theoretical pictures of the 2D turbulence. The results suggest that the computational complexity of 2D turbulent flows may be reduced in simulations by considering only coherent structures interacting with a statistically modeled background.

Contents

[1] Author to whom any correspondence should be addressed.

1. Introduction

The laboratory investigation of two-dimensional (2D) Eulerian flows is a challenging task. Experiments performed with rotating tanks [1], soap films [2] or thin electrolyte layers [3, 4] are always affected by non-ideal effects and deviations from two dimensionality. This makes the comparison with theoretical models difficult. On the other hand, highly magnetized pure electron plasmas confined in Malmberg–Penning traps [5] allow one to perform experiments on 2D fluid dynamics, where these non-ideal effects can be drastically reduced. In fact, under suitable experimental conditions the transverse dynamics of the electron plasma in the trap is well described by the drift-Poisson system [6, 7] (cold non-relativistic guiding center approximation):

$$\partial n/\partial t + \vec{v}\cdot\nabla n = 0, \quad \vec{v} = -\nabla\phi\times\vec{e}_z/B, \quad \nabla^2\phi = en/\epsilon_0, \tag{1}$$

where n is the plasma density, ϕ the electrostatic potential, B the magnetic field, $\vec{v}$ the velocity field, $-e$ the electron charge, ϵ_0 the vacuum permittivity and $\vec{e}_z$ the unit vector in the axial direction. Equations (1) are isomorphic to the Euler equations for an ideal (incompressible, inviscid) fluid, with vorticity $\zeta = en/\epsilon_0$ and stream function $\psi = \phi/B$. In the electron plasma case, no boundary layer exists, free-slip boundary conditions hold, the velocity field is divergence free and viscosity effects (mainly due to collisions of the electrons with the residual neutral gas) become negligible under ultra high vacuum conditions. For a residual gas pressure of 10^{-9}–10^{-8} mbar, the kinematic plasma viscosity (estimated from elastic electron–neutral collision at the Larmor radius scale) is of the order of 10^{-5}–$10^{-4}\,\mathrm{m^2\,s^{-1}}$, and effective Reynolds numbers up to $Re \approx 10^5$ can easily be reached [8].

There exists a solid theoretical foundation for 2D isotropic and homogeneous turbulence [9, 10]. The dynamical equations and statistical-mechanical behavior, both equilibrium and non-equilibrium, of turbulent 2D flows described by either continuous vorticity distributions or by the interaction of collections of discrete vortices, is reviewed, e.g., in [11]. These classical treatments in turbulence strongly rely on the use of the Fourier representation. On the other hand, in a 2D turbulent fluid long-lived coherent structures with different space scales develop even at very high Reynolds numbers, breaking the homogeneity hypothesis [12]. The analysis of the turbulence, performed on the basis of the experimental data, should then be able to discriminate the coherent and the incoherent parts of the flow. For this reason, in the present paper wavelet transforms [13] are used, which, contrary to Fourier transforms, have well-localized basis functions both in physical and 'wave-number' space (see e.g. [14] and references therein). Although the Fourier analysis leads to good results in many cases, some disadvantages are present. For example, in the simple case of a 1D signal the information concerning time variations (for instance, a discontinuity or a localized high variation of the frequency of the signal) is lost in the Fourier description. This is due to the nature of the functions (complex exponentials) used as basis functions, which cover the entire real line. In contrast, wavelets are able to restore time location as well as frequency informations [15]. For the case of homogeneous and isotropic turbulence, Fourier and wavelet methods give equivalent results for the power spectra (see e.g. in a different context [16]). In the present case of 2D turbulence in an electron plasma, the presence of localized coherent structures introduces non-negligible contributions at all scales (wavenumbers) in the Fourier space, determining a piling-up effect at small spatial scales, so that the Fourier analysis is no longer a proper inspection tool.

In the case of non-neutral plasmas, the late time dynamics of a free decaying 2D turbulence has been analyzed using variational methods [17], to explain the formation of vortex crystal

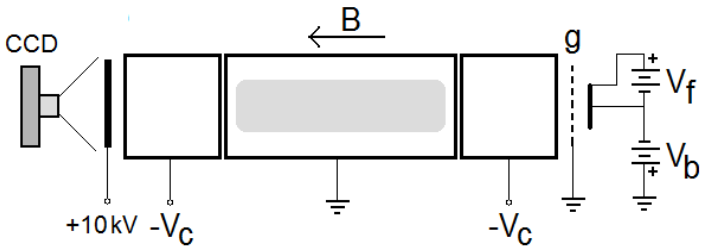

Figure 1. Schematic of the Malmberg–Penning trap ELTRAP. A low density ($n = 10^{12}$–$10^{13}\,\mathrm{m}^{-3}$) and temperature ($T = 1$–$10\,\mathrm{eV}$) electron plasma is generated by a thermionic cathode heated with a constant current and biased with respect to a grounded grid (g). The voltage drop across the filament, V_f, and the source bias, V_b, set the initial plasma radius and density. The electrons are axially trapped within a stack of hollow conducting cylinders (with radius $R_W = 4.5\,\mathrm{cm}$) by two fixed voltages $-V_c$, and radially confined by an axial magnetic field B which keeps the charged column in equilibrium rotation. In the experiments described in the paper the plasma length is about 50 cm, the magnetic field is $B = 0.167\,\mathrm{T}$, and the neutral gas pressure is $p \approx 5 \times 10^{-9}$ mbar.

states [18], while the early stage has been studied in terms of the time behavior of the number of coherent vortices [19]. More recently, a spectral analysis of the evolution of an electron plasma has been performed with the Fourier transform [20]. A first preliminary comparison between Fourier and wavelet analysis of a turbulent electron plasma has been described in [21, 22]. In a very recent paper [23], a wavelet analysis of the system studied in [20] has been performed in order to identify the spectra of the coherent and the incoherent parts of the flow.

Here a detailed wavelet analysis of the turbulence of an electron plasma is presented, performed on the basis of a directly measured (axially averaged) density distribution. The wavelet spectra of enstrophy and energy, and their temporal evolution, have been obtained both for the coherent and the incoherent parts of the flow. Scale contributions to the measured enstrophy and energy distributions are inferred. The wavelet technique allows the separation of two 'structures': the solid rotation part of the vortices and the remaining part, mainly composed of vorticity filaments. In particular, it is found that the incoherent component does not contribute significantly to the dynamical properties of the 2D electron plasma flow, and is characterized by a near Gaussian vorticity PDF and an increasing spatial wavenumber spectrum. The results appear to be in qualitative agreement with numerical simulations of 2D turbulence in circular domains reported in the literature [24]–[27], while some points of disagreement are evidenced with the results presented in [23].

The following two sections refer to the experimental results and the wavelet analysis of the data. Short conclusions are contained in the last section.

2. Experimental results

The experimental data reported in the present paper have been obtained in the Malmberg–Penning trap ELTRAP [28]. In figure 1, a simplified schematic of the device is shown. The time evolution of the system is monitored through an optical diagnostic system. The device operates according to an injection–hold–dump cycle [28]: the electron plasma is

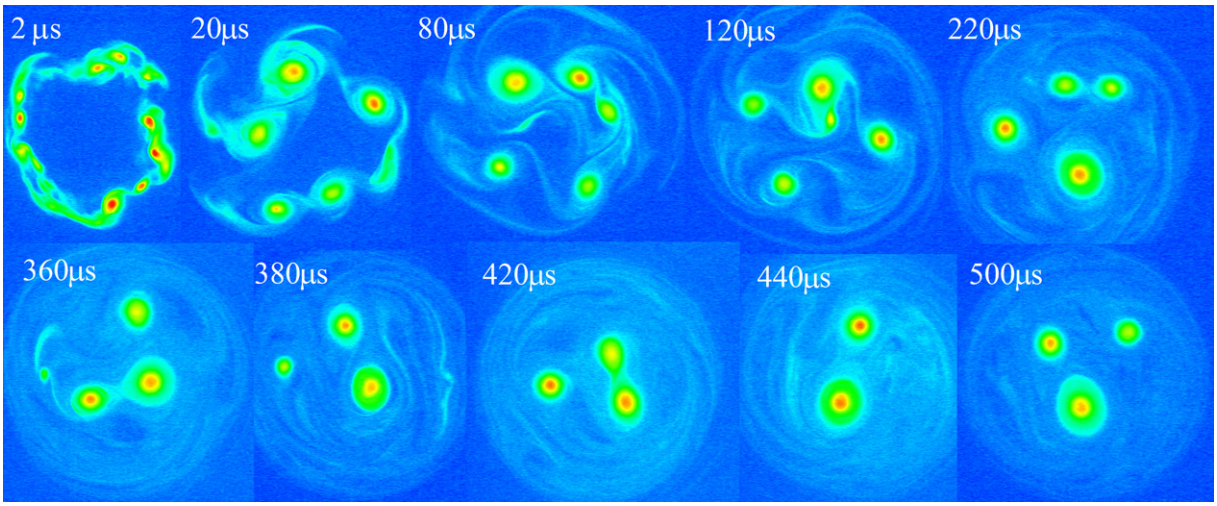

Figure 2. Evolution of the plasma: the trapping time is indicated at the top left corner of each frame.

trapped for a given time, then dumped onto a phosphor screen. The light emitted by the screen is collected by a 12 bit charge-coupled device (CCD) camera. The intensity of the light on a given point on the snapshot is proportional to the axially averaged plasma density. Several machine cycles are repeated keeping the injection parameters fixed and increasing the trapping time. The shot-to-shot reproducibility of the plasma initial conditions is very high: the variation of the measured charge at a given point and time is typically less than 0.1%, in agreement with previous experiments on electron plasmas.

A typical plasma evolution is shown in figure 2. The first frame (corresponding to a trapping time $\tau = 2\,\mu$s) reflects the shape of the spiral cathode distorted by the diocotron [6] (or Kelvin–Helmholtz in the fluid case) instability, which rapidly leads to a highly nonlinear evolution of the flow. Several small vortices form, which then interact through close encounters resulting in merger events and emission of vorticity filaments, and leading eventually to the formation of a diffuse background. At $\tau = 500\,\mu$s the plasma has reached an almost azimuthally symmetric, monotonically decreasing radial density profile, in which all the small scale structures have been smeared out.

3. Multiresolution analysis

The method described in [25] is applied here in order to separate the coherent structures from the incoherent vorticity distribution with the minimum degree of arbitrariness (e.g. without density cutoff) and perform a separated spectral analysis on the coherent and incoherent parts of the flow.

A multiresolution analysis [29] is used, which successively decomposes the signal into coefficients that contain coarse and fine details at increasingly finer resolution. The 2D vorticity field is expanded as

$$\zeta(x, y) = \bar{\zeta}_{0,0,0}\phi_{0,0,0}(x, y) + \sum_{j=0}^{J-1}\sum_{i_x=0}^{2^j-1}\sum_{i_y=0}^{2^j-1}\sum_{\sigma=1}^{3}\tilde{\zeta}^{\sigma}_{j,i_x,i_y}\psi^{\sigma}_{j,i_x,i_y}(x, y), \tag{2}$$

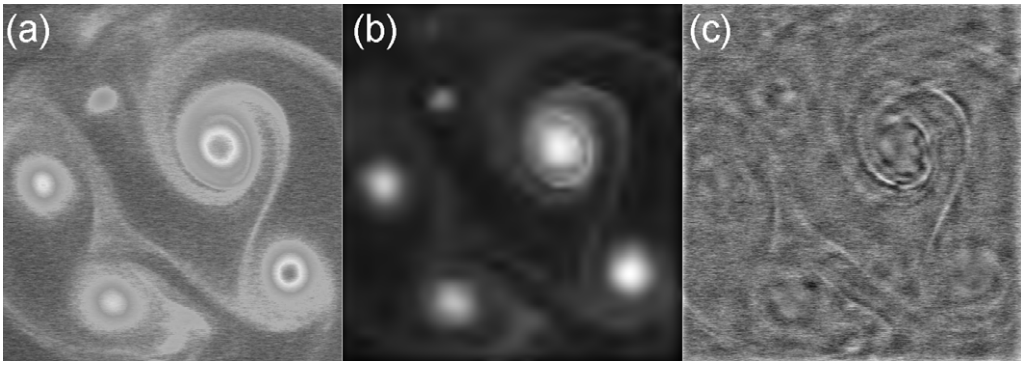

Figure 3. Left: details of the density (vorticity) distribution at $\tau = 90\,\mu$s. Center: reconstructed coherent flow with nonlinear wavelet thresholding. Right: incoherent flow.

i.e. as a linear combination of elementary well-localized functions $\psi^{\sigma}_{j,i_x,i_y}(x,y)$, weighted by the wavelet coefficients $\tilde{\zeta}^{\sigma}_{j,i_x,i_y}$. These are calculated on a dyadic grid as cross-correlation values between the signal and the mother wavelet $\psi(x,y)$, expanded by a factor 2^{-j} ($j = 0,\ldots,J-1$) and translated on the grid ($2^J \times 2^J$ represents the number of data). Here $\phi_{j,i_x,i_y}(x,y) = \phi_{j,i_x}(x)\phi_{j,i_y}(y)$, $\psi^{\sigma=1}_{j,i_x,i_y}(x,y) = \psi_{j,i_x}(x)\phi_{j,i_y}(y)$, $\psi^{\sigma=2}_{j,i_x,i_y}(x,y) = \phi_{j,i_x}(x)\psi_{j,i_y}(y)$ and $\psi^{\sigma=3}_{j,i_x,i_y}(x,y) = \psi_{j,i_x}(x)\psi_{j,i_x}(x)$, where $\phi(\cdot)$ and $\psi(\cdot)$ are the 1D scaling function and the associated wavelet, respectively. Due to the orthogonality of the wavelet functions, the decomposition conserves the total enstrophy $Z = (1/2)\int \mathrm{d}^2 r \zeta^2$.

In [25] coherent structures were evidenced from the numerically computed turbulent flow using an adaptive, self-consistent universal Donoho's threshold [30] within an iterative method. In practice, wavelet coefficients at a given iteration step are divided into coefficients smaller and greater (in absolute value) than a threshold $\epsilon^{(j)} = \sqrt{2\sigma^{2(j)} \ln N^{(j)}}$. Inverse transforming one obtains $\zeta^{(j)}_{<}$, the incoherent flow, and $\zeta^{(j)}_{>}$, the coherent flow at the iteration step j. $N^{(j)}$ is the number of data contained in $\zeta^{(j)}_{<}$, and $\sigma^{2(j)}$ the variance of $\zeta^{(j)}_{<}$. At the first iteration, $\sigma^{2(0)}$ is the variance of the whole signal $\zeta(x,y)$ (overestimated variance), and $N^{(0)}$ is the total number of data. After a few iterations, the threshold stabilizes (indicating convergence) and the coherent and the incoherent flows are separated. The efficiency of the algorithm described above does not depend on the wavelet choice, provided that it is smooth enough and has a high enough number of vanishing moments. Here the Symlet8 wavelet, similar to the quintic spline used in [25], has been chosen.

It is important to note that for the analysis of the experiments also the image in the absence of the plasma (which is usually subtracted from the raw data) has to be processed, because it contains an intrinsic noise contribution which cannot be associated with any real flow. This 'dark image' is separated into a coherent contribution, due to the fixed residual background light, and an incoherent one, due to noise that is thermally generated inside the CCD camera. After the fixed light contribution has been subtracted from the raw intensity data, the iterative eduction is applied, obtaining the coherent flow $\zeta_{>}$. It has been verified that the instrumental noise due to the dark current gives a negligible contribution to the total incoherent signal energy.

Calculations are performed on the data belonging to the sequence shown in figure 2. A typical result of the fractioning algorithm is shown in figure 3, which refers to the vorticity

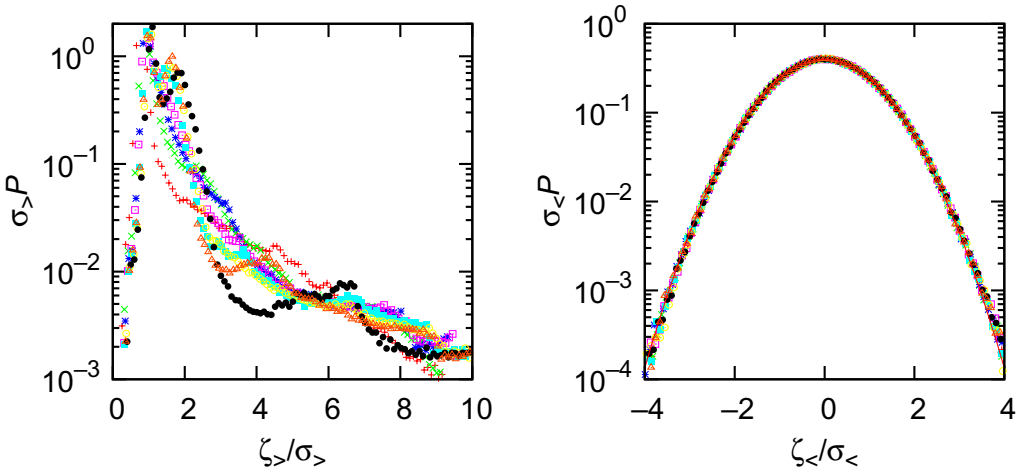

Figure 4. PDF of the coherent (left) and the incoherent (right) part of the flow (multiplied by the respective variances) for different trapping times: $\tau = 2\,\mu$s (plus symbols, red), 20 μs (asterisks, blue), 40 μs (crosses, green), 80 μs (open triangles, orange), 200 μs (open squares, violet), 300 μs (full squares, light blue), 400 μs (open circles, yellow) and 500 μs (full circles, black). The solid line represents a Gaussian fit of the 2 μs curve.

distribution at $\tau = 90\,\mu$s. The coherent flow $\zeta_>$ has been reconstructed by means of a small fraction of the wavelet coefficients ($\simeq$1.1%) but it contains the greatest part of the signal energy (99.3% of the total enstrophy). Conversely, the incoherent flow $\zeta_<$ contains the majority of the wavelet coefficients but only a very small fraction of the total signal energy. It is observed from figure 3 that the coherent part of the flow (corresponding to the strongest wavelet coefficients) is composed of vortices, while the incoherent part (corresponding to the weakest coefficients) is mainly composed of vorticity filaments.

The probability distribution functions (PDFs) of the flow for different times are shown in figure 4. It is worth noting that the PDF of the incoherent flow does not depend on the spatial configuration of the coherent flow and remains Gaussian to a very good approximation (the excess kurtosis ranges from -0.012 to 0.047, and the skewness from 0.013 to 0.032). In contrast, the PDFs of the coherent structures vary in time, depending on their spatial distribution, indicating that they are out of equilibrium. This result agrees with the numerical simulations reported in [25].

The stability of the PDF of $\zeta_<$ found in the experiments enforces the hypothesis that in the turbulence modeling there is separability among a set of active modes, or strong wavelet coefficients, and passive modes, the weak wavelet coefficients. In other words, while the evolution of coherent structures has to be directly computed, the background of vorticity is only advected and mixed by the strain imposed by the coherent vortices and can be statistically modeled through its stationary PDF. This assumption has been used in the coherent vortex simulations method described in [25] in order to reduce the computational effort (degrees of freedom of the flow). In that case the reliability of the results is based on the comparison with direct numerical simulations of 2D Navier–Stokes equations, with intrinsic limitations due to the fast growing computational cost for increasing Reynolds number ($\propto Re$ in two dimensions), but sufficient experimental proof is still lacking. In the experiment reported here the reduction

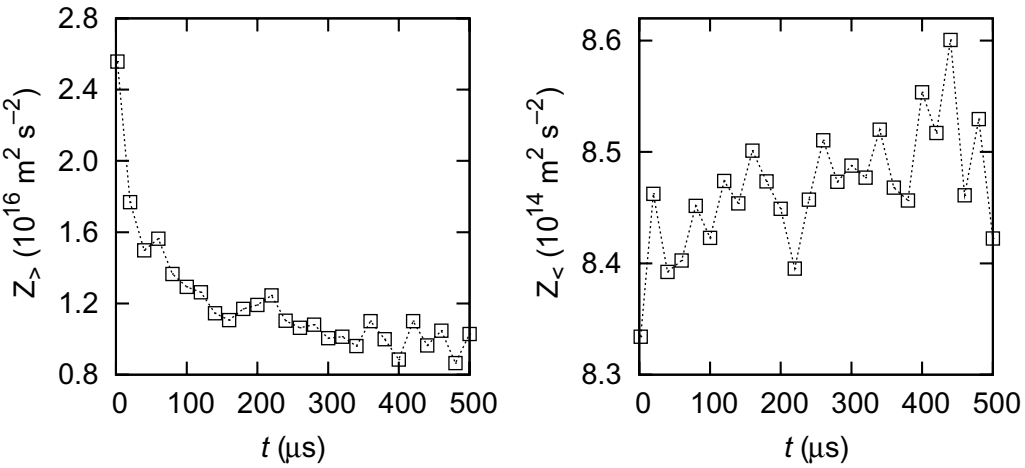

Figure 5. Time evolution of the coherent ($Z_>$, left) and the incoherent ($Z_<$, right) part of the total enstrophy for the time sequence of figure 2.

of degrees of freedom is indicated by the high compression factor of the signal energy (see figure 3), and by the stability of the PDF of the residual coefficients.

The contribution of the coherent and incoherent components of the flow to the total enstrophy and energy have been analyzed. The total enstrophy $Z(t)$ decreases in time, and rapidly reaches about one-half of its initial value, as shown in figure 5. Although enstrophy and all higher moments of vorticity are conserved by the 2D Euler equations, their measured values are generally not conserved in freely relaxing 2D turbulence. This is because any physical measurement of vorticity at a given position is an average over a cell of small but finite area. As vorticity filaments stretch and their thickness becomes smaller than the experimental resolution (CCD pixel size), the corresponding measured vorticity decreases. In this sense, enstrophy and all higher moments are 'fragile' invariants, and their measured values will decrease with time due to coarse-graining. This behavior has been observed previously both in experiments and in numerical simulations [8]. Many papers on the statistical mechanics of 2D turbulence also discuss the effect of coarse-graining on the integral invariants of 2D Euler flow (see e.g. [31]).

The spectral analysis (see figure 6), although limited in resolution by the small number of scales imposed by the orthogonality of the discrete wavelet transform, evidences that most of the enstrophy is contained in long wavelengths (small k). This is consistent with the observation of the vorticity (density) fields and the persistence of structures with large amplitude vorticity.

Figure 7 shows the spatial distribution of the enstrophy at different scales for a trapping time $\tau = 2\,\mu$s. The maximum content of enstrophy is found in plot (b), corresponding to $n = 6$ and to a scale length of the order of 5 mm. This corresponds to the maximum of the enstrophy spectrum for the coherent part of the flow in figure 6 at $k \sim 300\,\mathrm{m}^{-1}$.

Note that the $\zeta_>(k)$ curves are successively lower, according to the measured total enstrophy behavior. It is also to be observed that the significance of the last point in the figure is questionable as it corresponds to a scale length which becomes comparable to the Larmor radius of the particles. At these scale lengths the description of the transverse electron plasma dynamics by means of the 2D drift-Poisson system is no longer valid.

The incoherent field contains negligible enstrophy at large scales (indicating the lack of large scale features), it shows no or only small structures, and represents the dominant

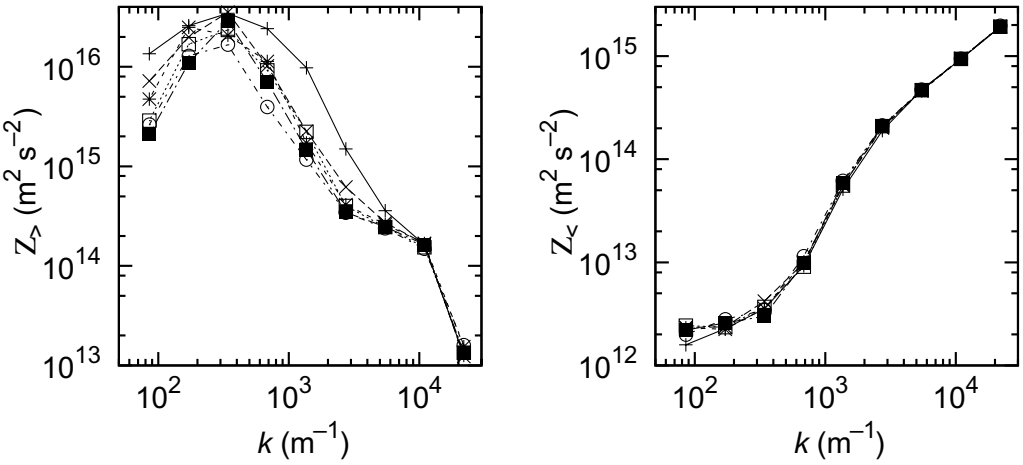

Figure 6. Spectral enstrophy distribution of the coherent flow (left) and of the incoherent flow (right) for $\tau = 2\,\mu$s (plus symbols), 20 μs (crosses), 40 μs (asterisks), 80 μs (open squares) and 200 μs (full squares).

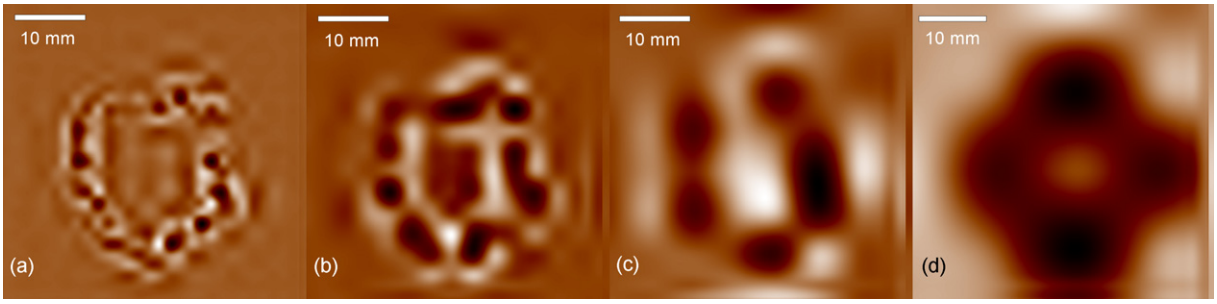

Figure 7. Spatial distribution of the enstrophy at different scales for $\tau = 2\,\mu$s (see figure 2). An inverted color palette is adopted, so that the maximum in each plot corresponds to the black dots. Panels (a), (b), (c) and (d) correspond to $n = 5$ (256 pixels of the original image), 6 (128 pixels), 7 (64 pixels) and 8 (32 pixels), respectively.

contribution to the enstrophy at large k. Three different scaling regions appear in the spectrum of the incoherent part. The first change of the slope is found to be related with the maximum enstrophy of the coherent part at the corresponding scale, which in turn is linked to the presence of the dominating coherent structures, as was shown above. The two spectra $\zeta_>(k)$ and $\zeta_<(k)$ show quite different scaling laws in the intermediate range $10^3 < k < 10^4\,\mathrm{m}^{-1}$, i.e. $\zeta_>(k) \propto k^{-1}$ while $\zeta_<(k) \propto k^2$. These scalings are consistent, e.g. with those found in [32], while they are in disagreement with the results presented in [23] obtained in an electron plasma confined in a Malmberg–Penning trap. One possible reason of this discrepancy may be the fact that the experiments reported in [23] are characterized by different plasma and geometric parameters than those reported here.

A wavelet spectral analysis has been performed also on the kinetic energy distribution of the flow, $(1/2)v^2(x, y) = (1/2)|\nabla\phi|^2/B^2$. In order to evaluate the kinetic energy density, the electrostatic potential $\phi(x, y)$ has been computed numerically starting from the measured

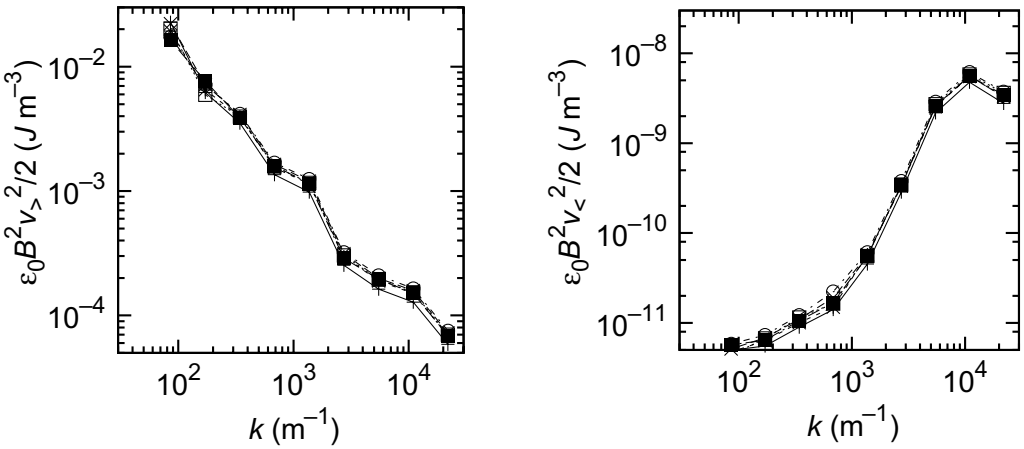

Figure 8. Spectral distribution of the kinetic energy of the coherent flow (left) and of the incoherent flow (right) for the same trapping times (and using the same symbols) as in figure 6.

2D electron density distribution on a square 940×940 Cartesian grid with zero boundary conditions at the circular wall radius, using a standard relaxation method. As in the case of the enstrophy, a separated spectral analysis has been performed on the coherent and incoherent density distributions, as shown in figure 8. In contrast to the enstrophy case, a very limited time evolution is found in the energy spectra due to a much smoother evolution of the electrostatic potential (from which the energy density is computed) with respect to the evolution of the density (from which the enstrophy density is computed). The coherent part of the flow evidences a k^{-1} scaling, whereas for the incoherent part a scaling approximately like k^3 is determined in the intermediate range $10^3 < k < 10^4\,\mathrm{m}^{-1}$. Note that unlike the enstrophy, the total energy of the flow is conserved with a relative accuracy better than 10^{-3}.

4. Conclusions

The experiments in a Malmberg–Penning trap show that 2D turbulent flows in a pure electron plasma are characterized by the presence of coherent vortices within a mixed, incoherent background. The discrete wavelet transform has been used to extract and study the dynamics of coherent structures. The flow has been separated into a 'coherent' and an 'incoherent' component using a self-consisting threshold of the coefficients of the discrete wavelet transform of the vorticity field (which is simply proportional to the density in a non-neutral plasma). A similar analysis has been performed for the kinetic energy spectra.

The presence of localized coherent structures in the flow introduces non-negligible contributions at all scales (wavenumbers) in the Fourier space. Not surprisingly, therefore, the wavelet spectra do not reproduce the classical results of Kraichnan and Batchelor [9, 10] obtained for a 2D homogeneous and isotropic turbulence.

Only 1.1% of the wavelet coefficients turns out to be necessary to represent the coherent component. The remaining small amplitude coefficients represent the incoherent component, which is characterized by a near Gaussian vorticity PDF. The wavelet-based separation of the flow into two dynamically different components therefore confirms that the computational

complexity of turbulent flows could be reduced in simulations by considering only coherent structures interacting with a statistically modeled incoherent background.

Acknowledgments

This work was supported by the Italian Ministry for University and Scientific Research 'PRIN-2007' funds.

References

[1] Baroud C N, Plapp B B, She Z and Swinney H L 2002 *Phys. Rev. Lett.* **88** 114501
[2] Rutgers M A 1998 *Phys. Rev. Lett.* **81** 2244
[3] Paret J and Tabeling P 1977 *Phys. Rev. Lett.* **79** 4162
[4] Rivera M, Vorobieff P and Ecke R E 1998 *Phys. Rev. Lett.* **81** 1417
[5] Malmberg J H and deGrassie J S 1975 *Phys. Rev. Lett.* **35** 577
[6] Levy R H 1965 *Phys. Fluids* **8** 1288
[7] Driscoll C F and Fine K S 1990 *Phys. Fluids* B **2** 1359
[8] Schecter D A, Dubin D H E, Fine K S and Driscoll C F 1999 *Phys. Fluids* **11** 4162
[9] Kraichnan R H 1967 *Phys. Fluids* **10** 1417
[10] Batchelor G K 1969 *Phys. Fluids* **12** II-233
[11] Kraichnan R H and Montgomery D 1980 *Rep. Prog. Phys.* **43** 547
[12] Frisch U 1995 *Turbulence: The Legacy of A N Kolmogorov* (Cambridge: Cambridge University Press)
[13] Grossman A and Morlet J 1984 *SIAM J. Math. Anal.* **15** 723
[14] Farge M 1992 *Ann. Rev. Fluid Mech.* **24** 395
[15] Mallat S G 1999 *A Wavelet Tour of Signal Processing* (San Diego: Academic)
[16] Katul G G, Parlange M B and Chu C R 1994 *Phys. Fluids* **6** 2480
[17] Jin D Z and Dubin D H E 1998 *Phys. Rev. Lett.* **80** 4434
[18] Fine K S, Cass A C, Flynn W G and Driscoll C F 1995 *Phys. Rev. Lett.* **75** 3277
[19] Jin D Z and Dubin D H E 2000 *Phys. Rev. Lett.* **84** 1443
[20] Kawai Y, Kiwamoto Y, Soga Y and Aoki J 2007 *Phys. Rev.* E **75** 066404
[21] Bettega G, Beretta D, Cavaliere F, De Luca F, Illiberi A, Pozzoli R, Romé M and Cavenago M 2007 Investigation of free decaying turbulence in a trapped pure electron plasma *Collective Phenomena in Macroscopic Systems* (Singapore: World Scientific) p 219
[22] Bettega G, Cavaliere F, Cavenago M, De Luca F, Pozzoli R and Romé M 2007 Experimental investigation of free decaying turbulence in a non-neutral plasma *Proc. 34th EPS Conf. on Plasma Physics (Warsaw, Poland) ECA* vol 31F (France: European Physical Society) p 2.099
[23] Kawai Y and Kiwamoto Y 2008 *Phys. Rev.* E **78** 036401
[24] Siegel A and Weiss J B 1997 *Phys. Fluids* **9** 1988
[25] Farge M, Schneider K and Kevlahan N 1999 *Phys. Fluids* **11** 2187
[26] Schneider K and Farge M 2005 *Phys. Rev. Lett.* **95** 244502
[27] Clercx H J H and van Heijst G J F 2000 *Phys. Rev. Lett.* **85** 306
[28] Amoretti M, Bettega G, Cavaliere F, Cavenago M, De Luca F, Pozzoli R and Romé M 2003 *Rev. Sci. Instrum.* **74** 3991
[29] Mallat S G 1989 *Trans. Am. Math. Soc.* **315** 69
[30] Donoho D L and Johnstone J M 1994 *Biometrika* **81** 425
[31] Miller J 1990 *Phys. Rev. Lett.* **65** 2137
[32] Schneider K, Farge M, Azzalini A and Ziuber J 2005 *J. Turbul.* **7** N44